Microfluidic Approach toward Continuous and Ultra-Fast Synthesis of Metal-Organic Framework Crystals and Hetero-Structures in Confined Microdroplets

Marco Faustini,[†§] Jun Kim,[‡§] Guan-Young Jeong,[†§] Jin Yeong Kim,[∥] Hoi Ri Moon,*[∥] Wha-Seung Ahn,*[‡] and Dong-Pyo Kim*[†]

[†] Department of Chemical Engineering, Pohang University of Science and Technology (POSTECH, Pohang, 790-784, Korea),

[‡] Department of Chemistry and Chemical Engineering, Inha University (Incheon, 402-751, Korea),

[∥] Interdisciplinary School of Green Energy, Ulsan National Institute of Science and Technology (UNIST, Ulsan, 689-798, Korea)

ABSTRACT: Herein, we report a novel nanoliter droplet-based microfluidic strategy for continuous and ultra-fast synthesis of metal-organic framework (MOF) crystals and MOF hetero-structures. Representative MOF structures, such as HKUST-1, MOF-5, IRMOF-3, and UiO-66, were synthesized within a few minutes via solvothermal reactions with substantially faster kinetics than the conventional batch processes. The approach was successfully extended to the preparation of demanding Ru_3BTC_2 structure that requires high-pressure hydrothermal synthesis conditions. Finally, three different types of core-shell MOF composites, i.e., Co_3BTC_2@Ni_3BTC_2, MOF-5@diCH_3-MOF-5, and Fe_3O_4@ZIF-8, were synthesized by exploiting a unique two-step integrated microfluidic synthesis scheme in a continuous flow mode. The synthesized MOF crystals were characterized by X-ray diffraction, scanning electron microscopy, and the BET surface area measurements. Compared with bare MOF-5, MOF-5@diCH_3-MOF-5 showed enhanced structural stability in the presence of moisture, and the catalytic performance of Fe_3O_4@ZIF-8 was examined using Knoevenagel condensation as a probe reaction. The microfluidic strategy allowed continuous fabrication of high quality MOF crystals and composites exhibiting distinct morphological characteristics in a time-efficient manner and represents a viable alternative to the time-consuming and multi-step MOF synthesis processes.

1. INTRODUCTION

Metal-organic frameworks (MOFs) are porous crystalline materials consisting of metal clusters or ions, which act as connecting nodes, and rigid organic bridging ligands. They have attracted immense attention because of their potential for extremely diverse structural topologies and tunable chemical functionalities.[1] Conventionally, MOFs are synthesized via time-consuming hydrothermal or solvothermal methods; these methods require several hours or days for crystallization and formation of the porous network. Other processes that involve alternative energy sources such as microwave irradiation or ultrasound significantly decreased the crystallization time and enabled control of morphology;[2] however, they often require special power-consuming apparatuses or set-ups. Fast formation of carboxylate-based MOFs crystals can also be achieved by the addition of nucleating agents,[3] deprotonation of the carboxylic acids at low temperature upon the addition of organic amines,[4,5] or the precipitation in suitable solvents such as in methanol,[6] which often leads to materials with reduced sorption properties. Despite these advancements, the development of continuous, faster, and viable processes for the synthesis of MOFs is still highly desirable for newly emerging commercial and industrial applications.

The utilization of microfluidic devices to confine reactants into nanoliter droplets has been extensively exploited for high-throughput biological and biochemical screening experiments over the last few decades.[7] Each microdroplet is essentially a miniature chemist's flask with the additional benefits of a high surface-area-to-volume ratio and highly efficient mixing and heat transfer; these characteristics usually lead to significantly enhanced reaction rates. Moreover, the use of microdroplets rather than continuous flow has proven to be particularly suitable for solid particles reagents because it can eliminate the channel clogging. This strategy has been adapted for the continuous synthesis of a wide spectrum of materials via polymerization,[8] precipitation, and sol–gel techniques.[9] Recently, hollow HKUST-1 microcapsules were also synthesized using an interfacial synthesis: the droplets act as a "liquid scaffold" to shape the material and the synthesis is driven by deprotonation of the carboxylic acid moieties at low temperature; unfortunately, the textural properties of products were inferior to conventionally synthesized HKUST-1.[4] The continuous solvothermal or hydrothermal synthesis of MOFs in microdroplets has not yet been reported.

This work presents the first comprehensive microfluidic strategy for ultra-fast and continuous synthesis of key MOF structures with homo- and hetero-compositions in confined

microdroplets. For this purpose, representative MOF structures of HKUST-1,[10] MOF-5,[1] IRMOF-3,[11] and UiO-66[12] were synthesized to demonstrate the feasibility and effectiveness of the microfluidic solvothermal process. The formation of high-quality crystals was realized within a few minutes; the reaction kinetics increased two orders of magnitude compared to the conventional solvothermal or hydrothermal batch processes. The microfluidic approach was then adapted for the preparation of Ru_3BTC_2 crystals, which requires high-pressure hydrothermal synthesis conditions. Finally, heterostructured MOF crystals comprising of core-shell or magnetic-core–MOF-shell composites were synthesized by a novel two-step serial microfluidic approach, which produced unique MOF structures with enhanced hydrostability or improved catalytic properties.

2. RESULTS AND DISCUSSION

Microfluidic System for Synthesis of MOFs. Figure 1 schematically illustrates the general set-up and procedure for the synthesis of MOF crystals using a microfluidic system. Initially, both organic and metal precursors are dissolved in a polar medium and then encapsulated in nanoliter droplets that are transported by the non-polar oil carrier. The microdroplets are generated by a T-junction polydimethylsiloxane (PDMS) chip device that is fabricated via a simple single-step scaffold method (Figure S1). The structure of the chip allows an easy and direct connection between the droplet generation device and the perfluoroalkoxyalkane (PFA) tubing, which prevent leakage and merging of the droplets. Subsequently, to conduct the solvothermal reaction for the synthesis of MOFs, the droplets that pass through the PFA tube are either immersed in a silicon oil bath or sent through an oven that was kept at the desired temperature (50−160 °C, Figures S2 and S3). The reaction time, which corresponds to the retention time of the droplets in the heating stage, was varied between 1 and 15 min by controlling the flow rates of the oil and polar solution phases. The precursor solution confined in the discrete nanoliter droplets and moved along the channel is subjected to highly efficient heat transfer in the droplets and chaotic advection that promotes mixing.[13] In addition, the high surface area to volume ratio of the confined environment also enhances heat and mass transfer leading to fast crystallization of MOFs in the droplets.[9] The in-droplet strategy does not only increase the crystallization kinetics but avoids channel clogging because of the absence of contact between the produced particles and the channel surface.

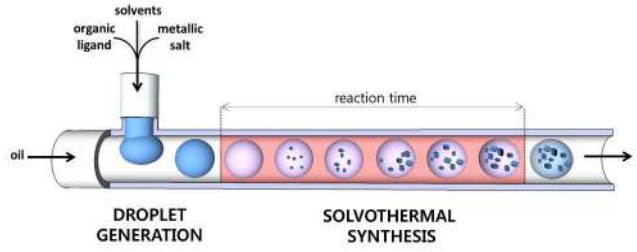

Figure 1. Schematic representation of general microchemical process.

Continuous Solvothermal Syntheses for MOFs: HKUST-1, MOF-5, IRMOF-3, and UiO-66. The validity of this microfluidic approach was first demonstrated through the synthesis of HKUST-1. Conventional solvothermal synthesis of this material usually requires treatment at 85 °C for 20 h.[14] In our experiment, the droplets containing copper nitrate and 1,3,5-benzene tricarboxylic acid (H_3BTC) dissolved in a DMF/H_2O/ethanol solvent were generated. Then, the droplets were conveyed into the microreactor loop and heated at 90 °C. Figures 2a−d (top) show optical images of single microdroplets taken through the PFA capillary after 1, 3, 6, and 12 min of synthesis. During the entire synthesis, the droplets maintained a uniform size (i.e., ~200 μm in lateral diameter). MOF crystals were clearly distinguishable inside the droplets even after only 1 min of reaction; the product yield increased with reaction time.

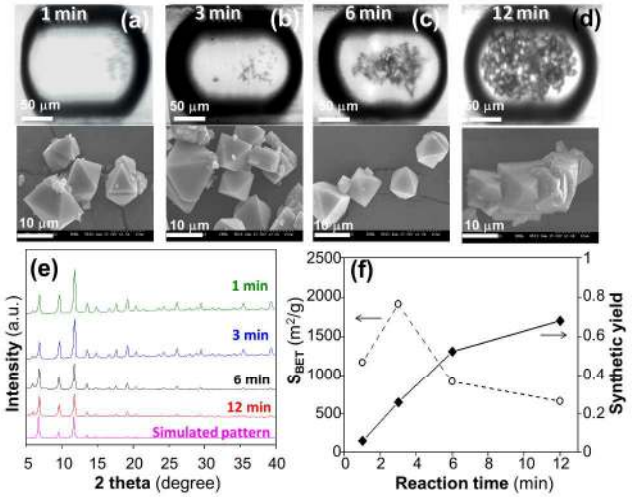

Figure 2. Optical and SEM micrographs of HKUST-1 crystals obtained via the microfluidic approach after (a) 1, (b) 3, (c) 6, and (d) 12 min of synthesis, [Cu] = 0.12 M. (e) The corresponding XRD patterns, which are compared with the simulated pattern from single-crystal XRD data of HKUST-1, and (f) the synthetic yield (bold line) and BET surface area, S_{BET} (dotted line) as a function of reaction time.

The morphology of the obtained crystals was investigated by scanning electron microscopy (SEM), as shown in Figures 2a−d (bottom): the particles consist of the typical 5−15 μm octahedral HKUST-1 crystals. The powder X-ray diffraction (XRD) patterns shown in Figure 2e confirm that the crystals obtained via the in-droplet microfluidic approach have the same crystal structure of HKUST-1 as those synthesized by the conventional solvothermal method (Figure S4, Table S1). The yield of the reaction, which is based on the copper content, is plotted as a function of the synthesis time in Figure 2f (bold line). The solid phase increases with reaction time: after 12 min, the synthetic yield was ca. 68%, which is similar to that obtained after 24 h via a conventional batch synthesis (65%). The production rate of HKUST-1 in the microfluidics system was estimated to be ~5.8 kg/m^3·day (Table S2), whereas small-scale laboratory syntheses described in the literature usually had a production rate lying between 0.1−1 kg/m^3·day.[15]

Standard N_2 adsorption measurements revealed that optimal BET surface area (1911 m^2 g^{-1}) was reached after 3 min of synthesis: in comparison, a conventional synthesis results in a BET surface area of 1664 m^2 g^{-1}. Increased synthesis time resulted in a decrease of the BET surface area. Another set of

experiments performed using a more concentrated ([Cu] = 0.60 M) precursor solution confirmed this trend (Figure S5 and S6). This behavior seems to reflect the intrinsic metastable nature of the MOF crystals, which can re-dissolve or degrade in the mother solution.[16]

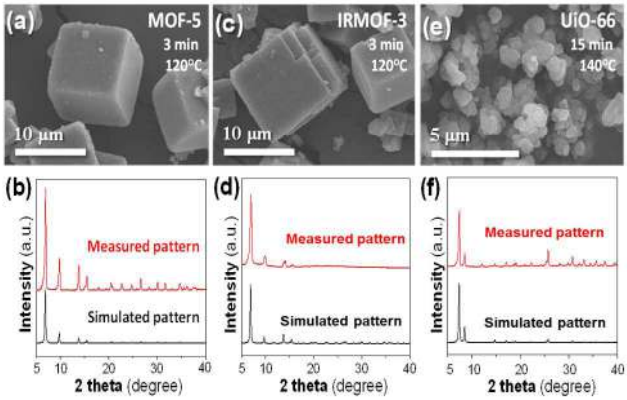

Figure 3. (a, c, and e) SEM micrographs and (b, d, and f) XRD patterns of (a and b) MOF-5, (c and d) IRMOF-3, and (e and f) UiO-66 crystals obtained via the microfluidic approach.

MOF-5 and IRMOF-3, which comprise Zn^{2+} with benzenedicarboxylate (BDC^{2-}) or 2-amino benzenedicarboxylate ($BDC\text{-}NH_2^{2-}$) ligand, respectively, were successfully synthesized in 3 min at 120 °C, as shown in Figures 3a and b, and c and d, respectively. UiO-66, which comprises Zr^{4+} and BDC^{2-}, was also successfully synthesized in the same device after 15 min at 140 °C, as shown in Figures 3e and f. The BET surface areas of MOF-5, IRMOF-3, and UiO-66 were 3185, 2428, and 1059 $m^2\ g^{-1}$, respectively, which were in agreement with the reported data.[1,11,12] MOF-5 and IRMOF-3 were cubic crystals in the size range of 10~15 μm that was obviously smaller than the conventional solvothermal products, but close in size to sonochemical products.[11,17]

Continuous Hydrothermal Synthesis under High Pressure: Ru_3BTC_2. A large number of MOFs are preparaed in water- or solvent-based systems in autoclaves above these boiling points to achieve high-pressure conditions. We were, therefore, motivated to extend the in-droplet microfluidic approach to the synthesis of MOFs that require harsher conditions, and selected Ru_3BTC_2 for our study, which has potentially interesting redox, photo-electrochemical and catalytic properties. The conventional synthesis of Ru_3BTC_2 involves the reaction of water-based mixtures of ruthenium chloride and H_3BTC in an autoclave for 72 h at 160 °C.[17] These conditions could not be directly applied to the aforementioned microfluidic system because H_3BTC is poorly soluble in water and a heterogeneous mixture containing organic powders can cause aggregation and subsequent channel clogging, which would prevent the generation of uniform droplets. Therefore, ethanol (10 wt%) was employed as a co-solvent to facilitate dissolution of the ligand. In addition, the process temperature required was high enough to cause evaporation of the solvent and resulting in the evolution of bubbles, which can lead to high back pressure and instability of the microfluidic system. The Ru_3BTC_2 synthesis was thus performed via a modified in-droplet microfluidic system under high-pressure hydrothermal conditions (Figures 4a and S3), in which the precursor solution and oil phase were injected using two high-pressure pumps. The generated droplets at a polytetrafluoroethylene (PTFE) T-junction were continuously flowed along PFA tubing that was placed in an oven at 160 °C. Solvent evaporation was avoided by fixing the injection pressure at 2.4 MPa via a back-pressure regulator (BPR). Under these conditions each droplet acted as a micrometer-scale autoclave in which MOF crystallizes.

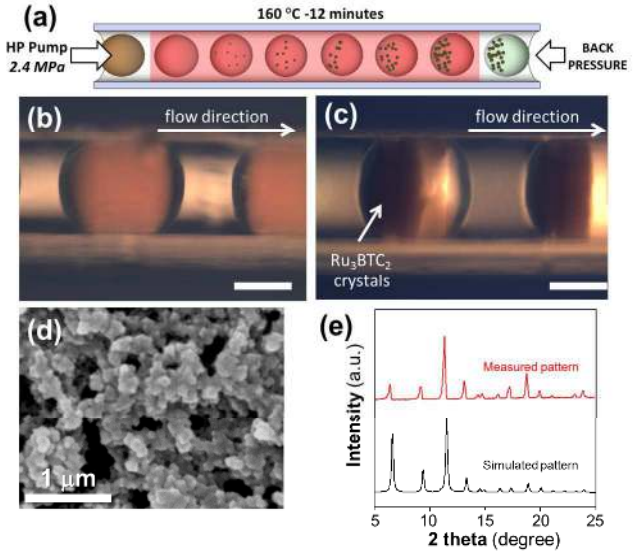

Figure 4. (a) Schematic representation of hydrothermal microchemical process. Optical images of single microdroplets containing (b) completely dissolved precursor solution and (c) segregated Ru_3BTC_2 crystals in the droplet after 12 min of synthesis at 160 °C and 2.4 MPa (scale bar: 100 μm). (d) SEM micrograph and (e) XRD pattern of the obtained crystals, which is compared with the simulated pattern from the single-crystal XRD of Ru_3BTC_2.

As shown in optical images of Figures 4b and c, the as-generated droplets displayed a homogeneous brown shade because of complete dissolution of ruthenium precursor. As the reaction proceeded, a dark-green product was observed and the droplet became bi-phased because of segregation of the product crystals at opposite ends of the droplet along the flow direction; no droplet merging or channel clogging occurred during 12 min of synthesis. The collected grey-green powders consisted of sub-micrometer crystals, as shown in the SEM micrograph in Figure 4d. The XRD pattern of the Ru_3BTC_2 sample (Figure 4e) shows the characteristic structure with a BET surface area of 550 $m^2\ g^{-1}$, and is in agreement with previous findings.[18]

Synthesis of Heterostructured MOFs via Two-Step Serial Microfluidic Approach: Co_3BTC_2@Ni_3BTC_2. The integrated core-shell MOFs are expected to have significant merits over individual MOF structures, because of synergistic effects such as enhanced structural stability, catalytic activity and adsorption properties.[19] In order to synthesize the core-shell MOFs via a step-wise serial process, the microfluidic system was extended by adding a second-capillary reactor to the end of the first one (Figure 5a). As a proof of the concept, a synthesis of Co-Ni core-shell MOF was initially synthesized to demonstrate the effectiveness of the hydrothermal droplet process employing serially connected microreactors (Figure

5b). The Co_3BTC_2 core crystals were first generated *in situ* during the residence of the droplet containing the core- precursor solution (i.e., cobalt(II) acetate tetrahydrate and H_3BTC dissolved in water) in the oil continuous phase for 5 min while flowing through an oven maintained at 140 °C. Subsequently, the droplets containing the Co_3BTC_2 core crystals were transported downstream into the second microreactor located in the same oven, after merging with the shell-precursors (i.e., nickel(II) acetate tetrahydrate and H_3BTC dissolved in water) at the T-scaffold junction. A BPR at the end of the microreactor was necessary to prevent solvent evaporation during the hydrothermal process (Figure 5a).

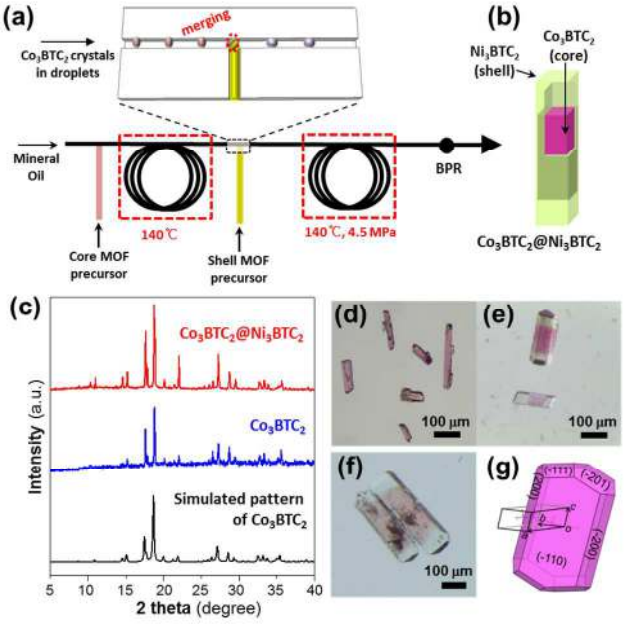

Figure 5. (a) A scheme of the integrated hydrothermal microchemical process for synthesis of core-shell MOFs. (b) Conceptual image of Co_3BTC_2@Ni_3BTC_2 core-shell MOF. (c) Experimental and simulated XRD patterns of the MOFs obtained via microfluidic approach. Optical images of (d) Co_3BTC_2 MOF crystals prepared at 140 °C for 5 min and (e) Co_3BTC_2@Ni_3BTC_2 core-shell MOF crystals prepared at 140 °C for 10 min. (f) Co_3BTC_2@Ni_3BTC_2 core-shell MOF crystals prepared by conventional hydrothermal method. (g) Simulated crystal morphology and crystallographic facets of Co_3BTC_2.

The conventional synthesis of Co and Ni MOFs reported by Yaghi *et al.*[20] was conducted using water-based mixtures of H_3BTC with cobalt(II) acetate tetrahydrate and nickel(II) acetate tetrahydrate, respectively, in an autoclave for 24 h at 140 °C. To the best of our knowledge, no attempt so far has been made to synthesize a Co_3BTC_2@Ni_3BTC_2 core-shell MOF by any means. The XRD patterns (Figure 5c) confirm that the Co_3BTC_2 products obtained via the in-droplet microfluidic approach after 5 min have the identical crystal structure as those synthesized by the conventional hydrothermal method. Moreover, the XRD pattern of the Co_3BTC_2@Ni_3BTC_2 core-shell particles produced via serial synthesis for total of a 10 min (i.e., two 5 min steps) was confirmed to be comprised of those of Ni_3BTC_2 and Co_3BTC_2 that were obtained by bulk syntheses (Figure S7). The morphology of the obtained crystalline particles was identified by optical microscopy (Figures 5d and e). The shape of both Co_3BTC_2 core and core-shell MOF crystals was cylindrical with high aspect ratios (length 60~150 μm, width 30~60 μm). In comparison, the conventional hydrothermal synthesis, which we performed, also successfully yielded Co_3BTC_2@Ni_3BTC_2 core-shell crystals; however, the reaction required ~72 h to complete, which included a series of heating, cooling, filtering, and washing steps. Using this method, the Co_3BTC_2 lost its single crystallinity because of the long heating period, as shown in Figure 5f. Therefore, the present two-step serial microfluidic method is a more reliable synthetic route to high-quality unstable and fragile materials.

The anisotropic crystal growth of Co_3BTC_2@Ni_3BTC_2 might be attributed to the elongated cell parameter of its core Co_3BTC_2 single crystal, which is monoclinic (a = 17.403, b = 12.958, and c = 6.477 Å). As shown in Figure 5g, simulation of the Co_3BTC_2 crystal morphology using the Bravais-Friedel-Donnay-Harker (BFDH) model revealed that its two-dimensional layers are infinitely stacked toward the c-axis, and the crystallographic c-axis runs parallel to the longest edge of the crystal.[21] This nature of the core crystal determines the isostructural growth of the shell MOF crystal; therefore the transparent Ni_3BTC_2 shell mainly grew at the ends of the Co_3BTC_2 crystal, which explains the observed epitaxial growth.

Synthesis of Heterostructured MOFs via Two-Step Serial Microfluidic Approach: MOF-5@diCH$_3$-MOF-5. MOF-5 has been extensively studied for applications in H_2 storage, gas separation, catalyst support, and sensing.[22] However, its lack of moisture stability, which is a consequence of the zinc-water coordination and simultaneous dissociation of the zinc-carboxylate bond via hydrolysis in the MOF-5 structure,[23] impairs its practical application. To resolve this problem, many attempts have been made to increase the water stability of MOF-5.[24] Recently, application of a hydrophobic methyl-functionalized BDC ligand, 2,5-dimethyl-benzene dicarboxylate (diCH$_3$-BDC), during the synthesis of MOF-5 was reported to yield an isostructural MOF that exhibited significantly enhanced stability in humid air.[24b] Unfortunately, its surface area and pore volume were decreased by ~30% relative to those of MOF-5 because the addition of methyl moieties to MOF-5 increases the unit mass and decreases the effective void volume. Accordingly, we envisaged that a MOF-5@diCH$_3$-MOF-5 core-shell structure that provides a thin shell as a water-resistant layer on the core MOF-5 may impart a high moisture stability with little deterioration of the textural properties. As shown in Figure 6a, this core-shell structure was prepared using the two-step serial microfluidic system; MOF-5@diCH$_3$-MOF-5 comprises two types of organic ligands in contrast to the previous example, which contained different metal ions in the core-shell MOF. Our serial microfluidic process not only dramatically reduced the reaction time, but also enabled effective protection of the MOF-5 core from exposure to moisture during handling, which is inevitable during the conventional two-step core-shell synthetic process.

The MOF-5 core was synthesized in 5 min using the procedure described earlier; then, diCH$_3$-MOF-5 shell was successively crystallized over the core in 15 min using diCH$_3$-BDC. Because of the identical colors of MOF-5 and diCH$_3$-MOF-5 crystals, MOF-5@diCH$_3$-MOF-5 core-shell structure was not

discernible as it is. Thus, the as-synthesized MOF-5@diCH$_3$-MOF-5 core-shell crystals were immersed in 94% ethanol to selectively destroy the core MOF-5 by exploiting the instability of MOF-5 toward water and alcohol molecules. As a result, the crystallinity of the core was lost by the diffusion of ethanol and water into the core-shell MOF. Eventually, the core became opaque while the shell maintained its transparency as shown at optical images of Figure 6a. This simple solvent treatment clearly established the successful synthesis of the MOF-5@diCH$_3$-MOF-5 core-shell structure. Quantitative analysis of the core and shell MOFs was performed using ^{1}H nuclear magnetic resonance (NMR) spectroscopy after digesting the synthesized MOF-5@diCH$_3$-MOF-5 core-shell in deuterated dimethyl sulfoxide (DMSO-d_6) prepared using diluted deuterium chloride (35% DCl in D_2O). The molar ratio of BDC/diCH$_3$-BDC was 3.7:1, revealing that the core was covered with a thin MOF shell (Figure S8).

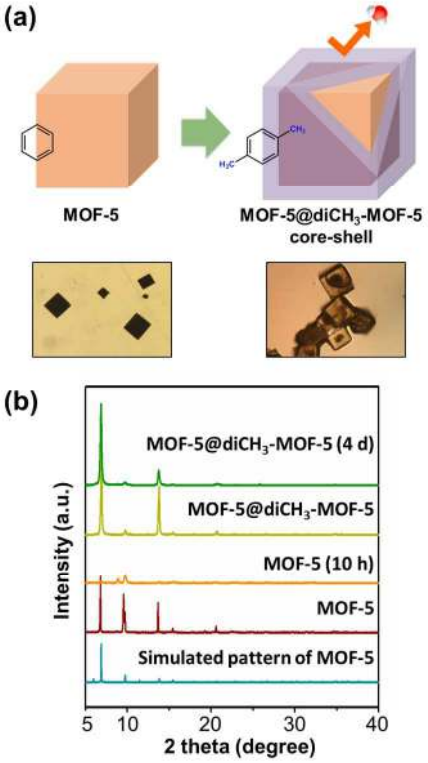

Figure 6. (a) Schematic view of the synthetic of MOF-5@diCH$_3$-MOF-5 core-shell structure and corresponding optical images after solvent treatment with ethanol. (b) XRD patterns of MOF-5 and MOF-5@diCH$_3$-MOF-5 core-shell MOF before and after exposure to humid air.

To examine the water stability of MOF-5@diCH$_3$-MOF-5, the guest DEF molecules occupied in the sample were first exchanged with volatile dichloromethane. This activated core-shell MOF was then exposed to ambient air with a relative humidity of 34−38%, and its stability was monitored by XRD. For comparison, bare MOF-5 was also examined via the same process. A new peak appeared in the XRD pattern of bare MOF-5 exposed to humid air after 2 h at 2θ=8.9^o, which corresponds to the hydrolyzed MOF-5;[23] the XRD pattern of the original MOF-5 mostly disappeared after 10 h (Figures 6b and S9). In contrast, the XRD pattern of the MOF-5@diCH$_3$-MOF-5 core-shell crystals did not change even after exposure to humidity for 4 d, which indicates significantly enhanced structural stability against moisture. Notably, no peak corresponding to the hydrolyzed MOF-5 appeared in the XRD pattern of MOF-5@diCH$_3$-MOF-5.

Synthesis of Heterostructures via Two-Step Serial Microfluidic Approach: Fe$_3$O$_4$@ZIF-8. Zeolitic imidazolate framework (ZIF) materials have zeolite-like topologies with interesting adsorption, separation and catalytic properties. Core-shell material composed of ZIF-8 (*sodalite* structure) on magnetic Fe_3O_4 particles was successfully prepared by the droplet microchemical process via a similar serial microfluidic process. The same composite material was also recently synthesized by the conventional solvothermal route.[25] The iron oxide precursor solution was prepared from $FeCl_3{\cdot}6H_2O$ with sodium acetate as a stabilizer and ethylene glycol as a reducing agent. Microfluidic droplets were created by separately injecting the Fe_3O_4 precursor solution and oil phase, and reacting the combined phases in an oven at 80 °C for 2 min. The generated in-droplet Fe_3O_4 particles were then transported downstream to the second microreactor to merge with a mixture of ZIF-8 precursor (i.e., zinc nitrate hexahydrate and 2-methylimidazolate dissolved in methanol) and polystyrenesulfonate for synthesis of the ZIF-8 shell at 50 °C; the Fe_3O_4 particles were firstly functionalized with the polystyrenesulfonate anion groups, then ZIF-8 was grown on the anion modified core particle. The XRD pattern in Figure 7a shows the successful synthesis of crystalline Fe_3O_4 at 80 ^{o}C after 2 min, which is consistent with spinel Fe_3O_4 phase (JCPDS 19-0629). In addition, the XRD pattern of Fe_3O_4@ZIF-8, obtained by heating at 50 ^{o}C for 5 min, shows the characteristic diffraction peaks of both materials. The SEM image in Figure 7b shows the spherical shape

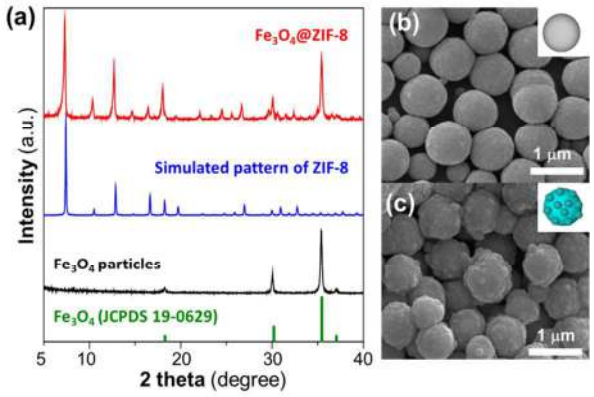

Figure 7. (a) XRD patterns of the obtained Fe_3O_4 and Fe_3O_4@ZIF-8 particles, which are compared with Fe_3O_4 (JCPDS 19-0629) and the simulated pattern of single-crystal XRD pattern of ZIF-8. SEM images of (b) Fe_3O_4, and (c) Fe_3O_4@ZIF-8 particles, synthesized at 80 ^{o}C for 2 min and 50 ^{o}C for 7 min, respectively.

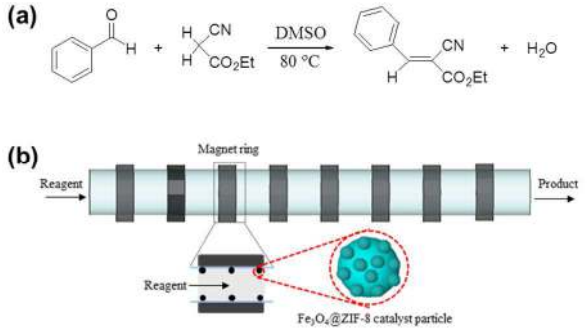

Figure 8. (a) Reaction scheme, and (b) microfluidic catalytic system for Knoevenagel condensation.

and smooth surface of the Fe_3O_4 particles, whereas the Fe_3O_4@ZIF-8 (size range 700 ± 50 nm) clearly depicts the presence of a ZIF-8 shell on the core magnetic particle (Figure 7c).

The catalytic efficiency of the as-synthesized particles was determined both in batch and PTFE capillary (1.6 mm od, 1.0 mm id, 100 cm length, Vici Co.) reactors to evaluate the performance of the core-shell Fe_3O_4@ZIF-8 particles. Knoevenagel condensation of benzaldehyde and ethyl cyanoacetate to yield ethyl (*E*)-α-cyanocinnamate was used as the model reaction (Figure 8a).[25,26]

At first, the catalytic reaction in the batch reactor was performed with simple mechanical stirring. The conversion of benzaldehyde was analyzed by gas chromatography/mass spectrometry (GC/MS) during reaction times of 5 to 50 min by tuning the flow rate: the conversion increased from 35% at 5 min to 49% at 50 min. The catalytic efficiency of the obtained Fe_3O_4@ZIF-8 was comparable to the reported values over the ZIF-8 catalyst synthesized by conventional bulk process for 12 h,[27] indicating no deficiency in the catalytic quality.

Since magnetic catalyst particles can be easily immobilized on the inside wall of the capillary microreactor by applying a magnetic field, the knoevenagel reaction was also conducted in the PTFE tubing by immobilizing the Fe_3O_4@ZIF-8 catalyst with a set of external magnet rings along the tube (Figure 8b). The conversion of benzaldehyde in the capillary reactor drastically increased from 55% at 5 min to 99% at 35 min of residence time (Figure S10). It is well-documented that the fast mass transfer and efficient diffusive mixing between the heterogeneous catalyst and reagent in the microreactor contribute toward a superior reaction performance to the bulk reaction.[28] The Fe_3O_4@ZIF-8 particles could be readily recovered with negligible loss from the solution using external magnets, as demonstrated in Figure S11.

3. CONCLUSIONS

In summary, we reported an ultra-fast and continuous synthesis microfluidic strategy as an alternative platform for preparation of versatile homo- and hetero-compositional MOFs with unique morphologies, which can be realized in confined droplets within a few min with reaction kinetics tremendously increased compared to the conventional batch processes. The effectiveness of this synthetic approach was demonstrated by efficient crystallization of representative MOF structures such as HKUST-1, MOF-5, IRMOF-3, and UiO-66 under diverse solvothermal conditions. The microfluidic approach was also applicable to the preparation of Ru_3BTC_2 crystals under high-pressure hydrothermal conditions. Eventually, unique hetero-structured Co_3BTC_2@Ni_3BTC_2, MOF-5@diCH_3-MOF-5 and Fe_3O_4@ZIF-8 core-shell MOF crystals were successfully synthesized using a novel two-step serial in-droplet microfluidic approach. Unique features such as anisotropic crystal growth or enhanced stability against moisture were observed in these MOFs. In addition, high quality of the prepared Fe_3O_4@ZIF-8 MOF particles and ease of separation were confirmed by observing reliable catalytic performances in the Knoevenagel condensation reaction. It is envisaged that the microchemical system can be scaled-up by designing high flows and multiple parallel microfluidic lines to meet the future industrial and commercial requirements.

4. MATERIALS AND METHODS

All chemicals used were analytical grade and used without further purification. All the inorganic precursors,1,3,5-benzene tricarboxilic acid (H_3BTC), 1,4-benzene dicarboxylic acid (H_2BDC), and 2-amino benzene dicarboxylic acid (H_2BDC-NH_2) were supplied by Aldrich. 2,5-dimethyl-benzene dicarboxylic acid (diCH_3-BDC) was purchased from TCI.

Characterization. Optical images of the droplets were takes through PFA tube with a Leika DMIL LED micrope. The scanning electron microscopy (SEM) was performed using a Hitachi S-4200. X-ray diffraction (XRD) data were obtained on a Rigaku diffractometer goniometer equipped with a CuKα (λ = 1.54 Å) radiation generator. The BET surface area and N_2 adsorption–desorption isotherms were measured at 77 K on a BELsorpII-mini using the Brunauer-Emmett-Teller (BET) method. Fourier−transform NMR spectra were measured using a Varian 600 MHz spectrometer.

Microfluidic Solvothermal Synthesis of HKUST-1. HKUST-1 precursor solution was prepared by adding $Cu(NO_3)_2{\cdot}H_2O$ and H_3BTC to a homogeneous solution of *N,N*-dimethylformamide (DMF), Ethanol (EtOH) and deionized water (H_2O) with a molar ratio $Cu(NO_3)_2{\cdot}H_2O/H_3BTC/H_2O/EtOH/DMF$ = 3:2:555:86:193. This mixture was stirred for 1 h until complete dissolution of the metallic salt and the organic ligand. The precursor solution was forced into the continuous phase at the T-junction of the channel to form the disperse phase; for the continuous phase, silicon oil (AP-150, Wacker) was introduced from the horizontal inlet. Both the dispersed and continuous phases were injected into the microfluidic device using a syringe pump (PHD 2000, Harvard Instruments, Holliston, MA). Each droplet reactor was then flowed along perfluoroalkoxyalkane (PFA) tube (i.d. 508 μm, length: 1.2 m), which was immersed in a silicon oil bath at 90 °C. The experiments were carried out at various flow rates of dispersed phase (Qd; 1-12 μL min^{-1}) and continuous phases (Qc; 5-60 μL min^{-1}) with constant ratio Qd:Qc = 1:5. After 1–12 min of reaction, the synthesized products were collected at the outlet of the PFA tube by a cooled vial at low temperature to avoid further crystallization. Then, the upper oil phase (continuous phase) was separated, and the synthesized products were collected by centrifuging (4000 rpm, 15 min). After washing several times the as-obtained samples with fresh EtOH, the resultant products were dried at 80 °C overnight under vacuum.

Microfluidic Solvothermal Synthesis of MOF-5 and IRMOF-3. MOF-5 precursor solution was prepared by adding $Zn(NO_3)_2{\cdot}6H_2O$ and H_2BDC to DMF, with a molar ratio $Zn(NO_3)_2{\cdot}6H_2O/H_2BDC/DMF$ = 3:1:270 (for IRMOF-3, H_2BDC-NH_2 was used instead of H_2BDC in the same precursor ratio of MOF-5). The mixture was synthesized by following the same procedure as HKUST-1 except for the temperature set at 120 °C. After 3 min of reaction, the synthesized products were collected at the outlet of the PFA tube, purified by centrifuging, washed 5 times with EtOH, and dried at 80 °C overnight under vacuum.

Microfluidic Solvothermal Synthesis of UiO-66. UiO-66 precursor solution was prepared by adding $ZrCl_4$, H_2BDC and HCl (37% in H_2O, Aldrich) to DMF, with a molar ratio $ZrCl_4/H_2BDC/HCl/DMF$ = 1:1:1:80. The mixture was synthesized by following the same procedure as HKUST-1 except for the temperature set at 140 °C. After 15 min of reaction, the synthesized products were collected at the outlet of the PFA tube, purified by centrifuging, washed 5 times with acetone, and dried at 70 °C overnight under vacuum.

Microfluidic Hydrothermal Synthesis of Ru_3BTC_2. Ru_3BTC_2 precursor solution was prepared as following: ruthenium chloride ($RuCl_3$) was dissolved in deionized water (H_2O) and, separately, 1,3,5-benzene tricarboxylic acid (H_3BTC) was dissolved in ethanol (EtOH). The dissolution rate of the organic ligand was enhanced by heating the mixture at 70 °C for 1 h. After dissolution the two solutions were mixed together in order to obtain a homogeneous and clear solution with molar composition $RuCl_3/H_3BTC/H_2O/EtOH$ = 3:2:2112:232. In order to stand the high pressure synthesis, a PTFE T-junction (Upchurch Scientific) was utilized to form the precursor solution droplets. Both the dispersed and continuous phases were injected into the microfluidic system using a high pressure pump (Primeline). Each droplet reactor was then flowed along PFA tube (i.d. 508 μm, length: 2 m), which was placed in an oven at 160 °C. A reaction time of 12 min was set by fixing the flow rates of both continuous and dispersed phases at 25 $\mu L\ min^{-1}$. The pressure of the microchemical system was adjusted by a back pressure regulator (Upchurch Scientific) in order to be equal to 2.4 MPa at the injection part. After reaction, the synthesized products were collected and treated by the same procedure as aforementioned.

Microfluidic Hydrothermal Synthesis of Co_3BTC_2. Co_3BTC_2 precursor solution was prepared by adding $Co(OAc)_2{\cdot}4H_2O$ (OAc = acetate), H_3BTC to H_2O, with a molar ratio $Co(OAc)_2{\cdot}4H_2O/H_3BTC/H_2O$ = 1.8:1:974. This mixture was sonicated for 0.5 h until the metallic salt and the organic ligand were well-dispersed in the solution. Dispersed solution was allowed to flow through a high pressure pump (Primeline) Note that stirring bar containing syringe and high pressure pump was vertically placed opposite to magnetic stirrer for continuous mixing of dispersed solution for homogeneous flow. The precursor solution was forced into the continuous phase at the T-junction of the channel to form the disperse phase; for the continuous phase, silicon oil (AP-150, Wacker) was introduced from the horizontal inlet. Both the dispersed and continuous phases were injected into the microfluidic unit. Each droplet reactor was then flowed along PFA tube (i.d. 800 μm, length: 1.2 m), which was immersed in a silicon oil bath at 140 °C. After 5 min of reaction, the resultant Co_3BTC_2 core crystals in-droplets were transported downstream into the second microreactor placed in the same oven to synthesize the shell material.

Microfluidic Hydrothermal Synthesis of Co_3BTC_2@Ni_3BTC_2 Core-Shell MOFs. Ni_3BTC_2 precursor solution was prepared by adding $Ni(OAc)_2{\cdot}4H_2O$, H_3BTC to H_2O, with a molar ratio $Ni(OAc)_2{\cdot}4H_2O/H_3BTC/H_2O$ = 17:1:46250. This mixture was sonicated for 0.5 h until complete dissolution of the metallic salt and the organic ligand. The precursor solution was merged into the as-obtained Co_3BTC_2 core crystals in-droplets at the T-junction of the channel to form the disperse phase. A BPR at end-side of microreactor were necessary to avoid solvent evaporation during hydrothermal process. After 5 min of reaction in a silicon oil bath at 140 °C, the synthesized core-shell products were collected at the outlet of the PFA tube, purified by centrifuging, washed 5 times with ethanol, and dried at 70 °C overnight under vacuum.

Microfluidic Solvothermal Synthesis of MOF-5@diCH_3-MOF-5 Core-Shell MOFs. The MOF-5 precursor solution was prepared by adding $Zn(NO_3)_2{\cdot}6H_2O$ and H_2BDC to *N,N*-diethylformamide (DEF) at a $Zn(NO_3)_2{\cdot}6H_2O/H_2BDC/DEF$ molar ratio of 11:3:333. The mixture was sonicated for 0.5 h until the metallic salt and the organic ligand were complete dissolved. The dispersed precursor solution was forced into the continuous phase at the channel T-junction at high pressure, while the continuous oil phase was introduced from the horizontal inlet. Both the dispersed and continuous phases were injected into the microfluidic unit and flowed along a PFA tube (i.d.: 500 μm, length: 1.5 m) immersed in a silicon oil bath at 100 °C. After 5 min of reaction, the resultant MOF-5 core crystals in-droplets were transported downstream into the second microreactor in the same oil bath to synthesize the shell material at the same temperature. The diCH_3-MOF-5 precursor solution was prepared by adding $Zn(NO_3)_2{\cdot}6H_2O$ and diCH_3-BDC to DEF at a $Zn(NO_3)_2{\cdot}6H_2O$/diCH_3-BDC/DEF molar ratio of 3:1:805. This mixture was sonicated for 0.5 h. The subsequent synthetic steps are the same as those for Co_3BTC_2@Ni_3BTC_2, except that BPR was not employed at the end of the microreactor. After 15 min of reaction, the synthesized core-shell products were collected at the outlet of the PFA tube (i.d.: 1 mm, length: 3.5 m).

Moisture Stability Study of MOF-5@diCH_3-MOF-5. The As-synthesized MOF-5@diCH_3-MOF-5 core-shell MOF crystals were immersed in anhydrous dichloromethane, which was replenished with a fresh solvent every 6 h, for 1 d. Solvent-exchanged core-shell MOF crystals were exposed to 34−38% humidity, and the structural stability was monitored by XRD.

Microfluidic Solvothermal Synthesis of Fe_3O_4. Fe_3O_4 precursor solution was prepared by adding $FeCl_3{\cdot}6H_2O$, NaOAc to ethylene glycol, with a molar ratio $FeCl_3{\cdot}6H_2O$/NaOAc/ethylene glycol = 1:7:80. This mixture was stirred for 0.5 h until complete dissolution. The precursor solution was forced into the continuous phase at the T-junction of the channel to form the disperse phase; for the continuous phase, silicon oil (AP-150, Wacker) was introduced from the horizontal inlet. Both the dispersed and continuous phases were injected into the microfluidic device at 80 °C. After 2 min of reaction, the synthesized Fe_3O_4 microspheres were transported downstream into the second microreactor placed in the same oven to synthesize the shell material.

Microfluidic Solvothermal Synthesis of Fe_3O_4@ZIF-8. ZIF-8 precursor solution was prepared by adding $Zn(NO_3)_2{\cdot}6H_2O$, 2-methylimidazolate, polystyrenesulfonate to methanol, with a molar ratio $Zn(NO_3)_2{\cdot}6H_2O$/2-methylimidazolate/polystyrenesulfonate/methanol = 1:10:20:1000. This mixture was stirred for 0.5 h until complete dissolution. The precursor solution was merged into the as-obtained Fe_3O_4 core crystals in-droplets at the T-junction of the channel to form the disperse phase. Both the dispersed and continuous phases were injected into the microfluidic device at 50 °C. After 5 min of reaction, the synthesized Fe_3O_4@ZIF-8 products were collected at the outer of the PFA tube, purified by external magnetic force, washed 5 times with ethanol, and dried at 70 °C overnight under vacuum for the characterization. **Catalytic Performance of Fe_3O_4@ZIF-8 for Knoevenagel Condensation**. In the case of capillary reactor, 10 mg of core-shell Fe_3O_4@ZIF-8 particles were immobilized on the inside wall of PTFE tubing with several sets of external magnet rings placed along the tube. Catalytic reaction in the batch reactor was performed with simple mechanical stirring using the same amount of catalyst. Both reactors were cleaned with ethanol 3 times. After cleaning, the reaction of equimolar benzaldehyde (1.0 mL, Sigma-Aldrich) and ethyl cyanoacetate (1.2 mL, Sigma-Aldrich) in DMSO (2 mL, Daejung chemicals) was performed at 80 °C. The residence time in the capillary reactor was varied from 5 min to 35 min by tuning the flow rates.

ASSOCIATED CONTENT

Supporting Information

Table S1 and S2, Figures S1−11. This material is available free of charge via the Internet at http://pubs.acs.org.

AUTHOR INFORMATION

Corresponding Author

dpkim@postech.ac.kr; whasahn@inha.ac.kr;
hoirimoon@unist.ac.kr

Author Contributions

[§]These authors contributed equally to this work.

Notes

The authors declare no competing financial interests.

ACKNOWLEDGMENT

This work was supported by the National Research Foundation of Korea (NRF) grant funded by the Korea government (MEST) (No. 2008-0061983). WSA also acknowledge a support from NRF (No. 2013005862).

REFERENCES

(1) Yaghi, O. M.; O'Keeffe, M.; Ockwig, N. W.; Chae, H. K.; Eddaoudi, M.; Kim, J. *Nature* **2003**, *423*,705.
(2) Choi, J.-S.; Son, W.-J.; Kim, J.; Ahn, W.-S. *Microporous Mesoporous Mater.* **2008**, *116*, 727.
(3) Falcaro, P.; Hill, A. J.; Nairn, K. M.; Jasieniak, J.; Mardel, J. I.; Bastow, T. J.; Mayo, S. C.; Gimona, M.; Gomez, D.; Whitfield, H. J.; Riccò, R.; Patelli, A.; Marmiroli, B.; Amenitsch, H.; Colson, T.; Villanova, L.; Buso, D. *Nat. Commun.* **2011**, *2*, 237.
(4) Ameloot, R.; Vermoortele, F.; Vanhove, W.; Roeffaers, M. B. J.; Sels, B. F.; De Vos, D. E. *Nat. Chem.* **2011**, *3*, 382.
(5) Li, H.; Eddaoudi, M.; O'Keeffe, M.; Yaghi, O. M. *Nature* **1999**, *402*, 276.
(6) Zhuang, J. L.; Ceglarek, D.; Pethuraj, S.; Terfort, A. *Adv. Funct. Mater.* **2011**, *21*, 1442.
(7) (a) Theberge, A. B.; Courtois, F.; Schaerli, Y.; Fischlechner, M.; Abell, C.; Hollfelder, F.; Huck, W. T. S. *Angew. Chem., Int. Ed.* **2010**, *49*, 5846. (b) Sharma, S.; Maurya, R. A.; Min, K. I.; Jeong, G. Y.; Kim, D. P. *Angew. Chem., Int. Ed.* **2013**, 52, 7564.
(8) Hoang, P. H.; Nguyen, C. T.; Perumal, J.; Kim, D. P. *Lab Chip.* **2011**, *11*, 329.
(9) Hoang, P. H.; Park, H. S.; Kim, D. P. *J. Am. Chem. Soc.* **2011**, *133*, 14765.
(10) Chui, S. S.; Lo, S.; Charmant, J. P. H.; Orpen, A. G.; Williams, I. D. *Science* **1999**, *283*, 1148.
(11) (a) Millward, A. R.; Yaghi, O. M. *J. Am. Chem. Soc.* **2005**, *127*, 17998. (b) Britt, D.; Tranchemontagne, D.; Yaghi, O. M. *Proc. Natl. Acad. Sci. USA* **2008**, *105*, 11623. (c) Gascon, F.; Aktay, U.; Hernandez-Alonso, M. D.; van Klink, G. P. M.; Kapteijn, F. J. Catal. **2009**, *261*, 75.
(12) Cavka, J. H.; Jakobsen, S.; Olsbye, U.; Guillou, N.; Lamberti, C.; Bordiga, S.; Lillerud, K. P. *J. Am. Chem. Soc.* **2008**, *130*, 13850.
(13) Song, H.; Chen, D. L.; Ismagilov, R. F. *Angew. Chem., Int. Ed.* **2006**, *45*, 733.
(14) Rowsell, L. C.; Yaghi, O. M. *J. Am. Chem. Soc.* **2006**, *128*, 1304.
(15) Czaja, A.; Leung, E.; Trukhan, N.; Müller, U. *Metal-Organic Frameworks: Applications from Catalysis to Gas Storage*; Farrusseng, D., Ed.; Wiley-VCH: Weinheim, 2011; p 344
(16) (a) Li, Z. Q.; Qiu, L. G.; Su, T.; Wu, Y.; Wang, W.; Wu, Z. Y.; Jiang, X. *Mater. Lett.* **2009**, *63*, 78. (b) Khan, N. A.; Jhung, S. H. *Bull. Korean Chem. Soc.* **2009**, *30*, 292.
(17) Son, W. J.; Kim, J.; Kim, J.; Ahn, W. S. *Chem. Commun.* **2008**, *47*, 6336.
(18) Kozachuk, O.; Yusenko, K.; Noei, H.; Wang, Y.; Walleck, S.; Glaser, T.; Fischer, R. A. *Chem. Commun.* **2011**, *47*, 8509.
(19) W. Zhang,; Q. Kuang,; J. Zhou,; X. Kong,; Z. Xie,; L. Zheng, *J. Am. Chem. Soc.* **2013**, *135*, 1926.
(20) Yaghi, O. M.; Li, H.; Groy, T. L. J. *J. Am. Chem. Soc*. **1996**, *118*, 9096.
(21) (a) Bravais, A. *Etudes Cristallographiques* (Paris: Gauthier Villars) **1866**. (b) Friedel, G. *Bull. Soc. Franc. Mineral*.**1907**, *30*, 326. (c) Donnay, J. D. H.; Harker, D. *Am. Mineral*. **1937**, *22*, 463.
(22) (a) Yang, J.; Sudik, A.; Wolverton, C.; Siegel, D. J. *Chem. Soc. Rev*. **2010**, *39*, 656. (b) Gallo, M.; Glossman-Mitnik, D. *J. Phys. Chem. C*, **2009**, *113*, 6634. (c) Sabo, M.; Henschel, A.; Fröde, H.; Klemm, E.; Kaskel, S. *J. Mater. Chem*., **2007**, *17*, 3827. (d) Halder, G. J.; Kepert, C. J.; Moubaraki, B.; Murray, K. S.; Cashion, J. D. *Science* **2002**, *298*, 1762.
(23) Kaye, S. S.; Dailly, A.; Yaghi, O. M.; Long, J. R. *J. Am. Chem. Soc*. **2007**, *129*, 14176.
(24) (a) Yang, S. J.; Choi, J. Y.; Chae, H. K.; Cho, J. H.; Nahm, K. S.; Park, C. R. *Chem. Mater*. **2009**, *21*, 1893. (b) Yang, J.; Grzeeh, A.; Mulder, F. M.; Dingemans, T. J. *Chem. Commun*. **2011**, *47*, 5244. (c) Chen, X.; Lukaszczuk, P.; Tripisciano, C.; Rummeli, M. H.; Srenscek-Nazzal, J.; Pelech, I.; Kalenczuk, R. J.; Borowiak-Palen, E. *Phys. Status Solidi B*, **2010**, *247*, 2664.
(25) Zhang, T.; Zhang, X.; Yan, X.; Kong, L.; Zhang, G.; Liu, H.; Qiu, J.; Yeung, K. L. *Chem. Eng. J*. **2013**, *228*, 398.
(26) Freeman, F. *Chem. Rev*. **1980**, *80*, 329.
(27) In this paper, authors achieved 55% conversion at 40 min for knoevenagel condensation of benzaldehyde and ethylcyano acetate in a batch reaction mode under the identical reaction conditions. See Tran, U. P. N.; Le, K. K. A.; Phan, N. T. S. *ACS catal*. **2011**, *1*, 120.
(28) Hoang, P. H.; Park, H. S.; Kim, D. P. *J. Am. Chem. Soc.* **2011**, *133*, 14765.

SUPPORTING INFORMATION

Microfluidic Approach toward Continuous and Ultra-Fast Synthesis of Metal-Organic Framework Crystals and Hetero-Structures in Confined Microdroplets

By *Marco Faustini*[‡1] *Jun Kim,*[‡2] *Guan-Young Jeong*[‡1]*, Jin Yeong Kim*[3]*, Hoi Ri Moon**[3]*, Wha-Seung Ahn**[2] and *Dong-Pyo Kim**[1]

[*] Prof. Hoi Ri Moon, Prof. Wha-Seung Ahn, Prof. Dong-Pyo Kim
[‡] These authors contributed equally
[1] Center of Applied Microfluidic Chemistry, Pohang University of Science and Technology, Department of Chemical Engineering, San31, Hyoja-dong, Nam-gu, Pohang 790-784, Korea
[2] Department of Chemical Engineering, Inha University, Incheon 402-751 , Korea
[3] Interdisciplinary School of Green Energy, Ulsan National Institute of Science and Technology (UNIST), UNIST-gil 50, Ulsan 689-798, Korea

E-mail: dpkim@postech.ac.kr, whasahn@inha.ac.kr, hoirimoon@unist.ac.kr

Fabrication of microfluidic droplet generator device

Microfluidic droplet generator devices with varying channel sizes were fabricated using polydimethylsiloxane (PDMS). The devices were made using a scaffold method without use of a photolithography master, as previously reported by our group.[S1] The template frameworks were assembled using commercially available tubes with different sizes purchased from Upchurch Scientific. First, the PFA tubing (o.d. ~1.5 mm, i.d. ~508 μm) was connected with both ends of polyetherether ketone (PEEK) tubing with an outer diameter (o.d.) of ~510 μm (Figure S1a). To create the perpendicular side channel for the droplet injection, another PEEK tube (o.d. 360 μm, i.d. 100 μm or 50 μm) was glued with horizontal PEEK tubing. This scaffold was then placed onto a Petri dish, and a mixture of a viscous PDMS precursor was then poured over the scaffold (Figure S1b). The system was left for degassing for 1 hour and cured for 1 hour at 70 °C. Finally, the border of the PDMS was cut by a blade and the template tubing was simply pulled out from the PDMS matrix leaving the T-junction channel structures behind (Figure S1c). The device was then directly connected to the PFA tube avoiding problems of leaking or droplet merging (Figure S1d).

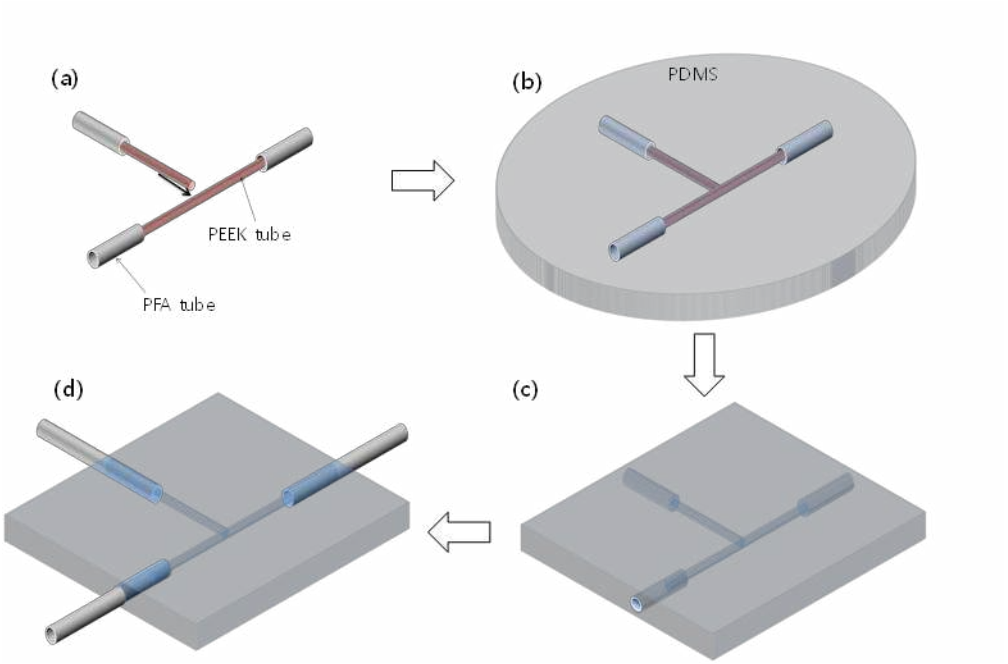

Figure S1. Schematic illustration of the fabrication process for the solvent resistant microfluidic droplet generator with different channel widths. (a) The PFA and PEEK assembly, (b) PDMS poured and cured into a petri dish. (c) Microfluidic device after removing the templates and (d) after connection with the tubes.

Microfluidic systems

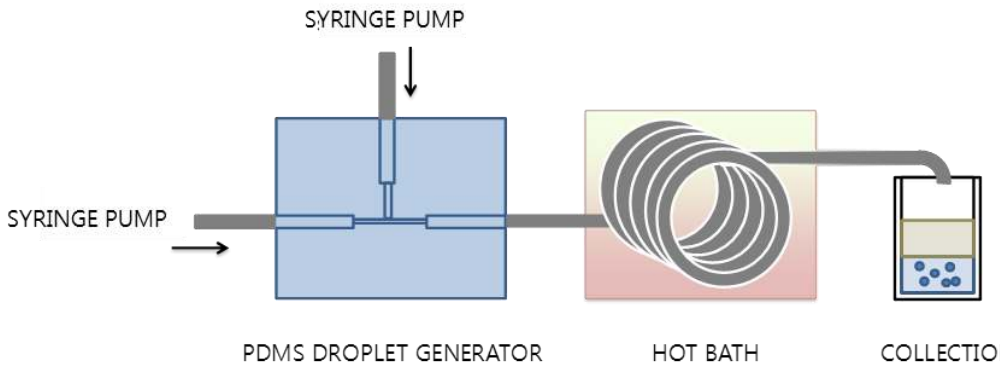

Figure S2. Microchemical system for solvothermal synthesis of HKUST-1, MOF-5 and UiO-66.

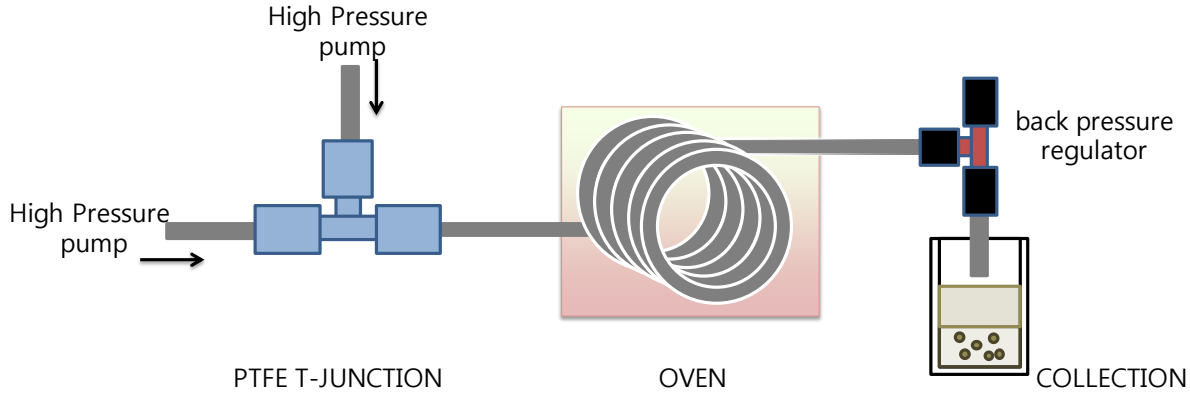

Figure S3. Microchemical system for hydrothermal synthesis of Ru_3BTC_2.

Microfluidic synthesis of HKUST-1

Table S1. Value of the specific surface area and pore volume of crystals obtained at different methods, reaction times, and concentrations.

Synthesis method	C_{Cu}[a] /mol L^{-1}	Oil flow rate / μL min^{-1}	PS[b] flow rate / μL min^{-1}	Reaction time / min	S_{BET}[c] / m^2 g^{-1}	V_{TOT}[d] / cm^3 g^{-1}
conventional	0.12			1440	1664	0.84
microfluidic	0.12	60	12	1	1171	0.62
microfluidic	0.12	20	4	3	1911	0.81
microfluidic	0.12	10	2	6	883	0.33
microfluidic	0.12	5	1	12	658	0.30
microfluidic	0.60	60	12	1	1105	0.62
microfluidic	0.60	20	4	3	1274	0.65
microfluidic	0.60	10	2	6	1958	0.82
microfluidic	0.60	5	1	12	851	0.33

[a] Cu^{II} concentration in precursor solution; [b] precursor solution; [c] BET surface area; [d] total pore volume.

Conventional synthesis (24 h) of HKUST-1

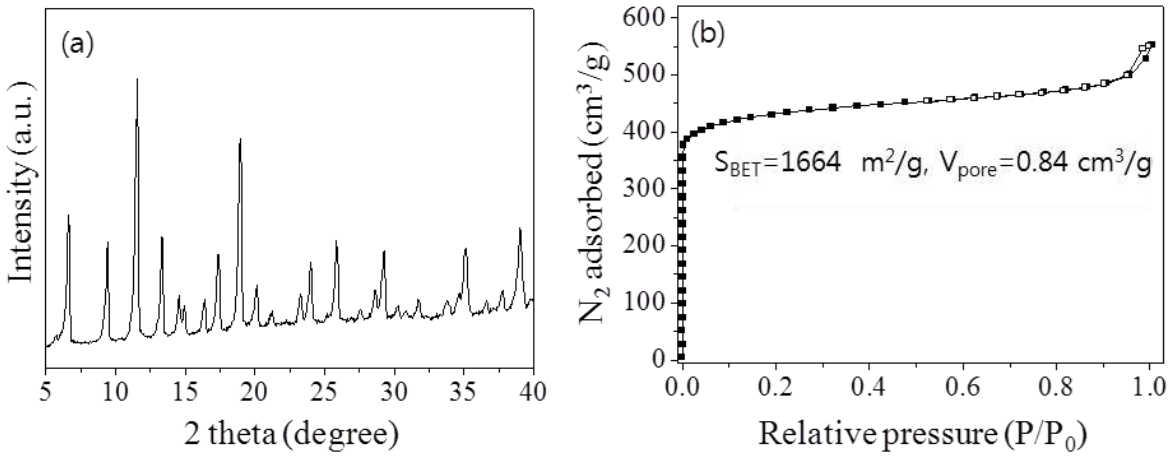

Figure S4. (a) X-ray diffraction pattern and (b) BET nitrogen sorption curve.

Calculation formula of the MOF production by the space-time yield (STY)

Table S2. Calculation formula table of the HKUST-1 production by the space-time yield (STY, kilograms of MOF product per cubic meter of reaction mixture per day).[a]

Flow rate / μL min^{-1}	Production rate / g day^{-1}	Calculation formula of conversion unit	Total production rate / kg m^{-3} day^{-1}
12	0.1	$\frac{0.1\ g/day\ \times 10^{-3} kg/g}{12\mu L/min \times 1440\ min \times 10^{-6} L/\mu L\ \times 10^{-3} m^3/L}$	5.8

[a] Microfluidic synthesis: ca. 0.1 g of HKUST-1 was produced after 24 h in a 12 μL/min of substrate flow. [Cu] = 0.60 M.

BET nitrogen sorption curves of HKUST-1 obtained by microfluidic approach

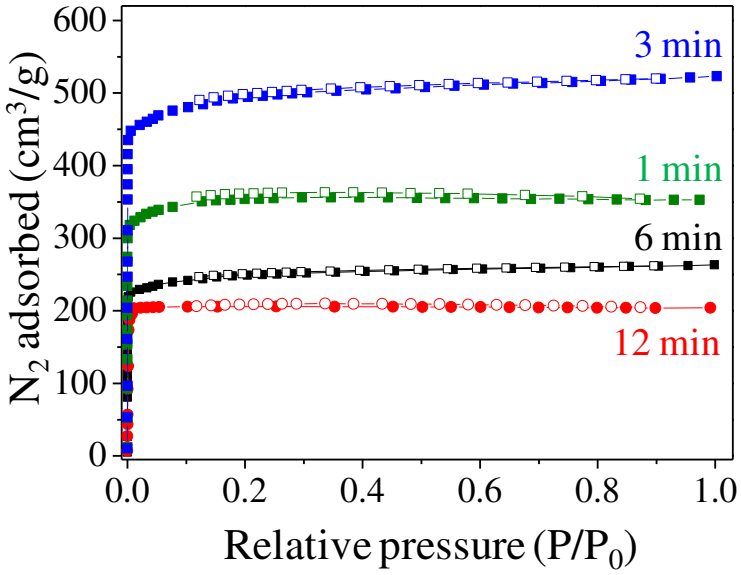

Figure S5. BET nitrogen sorption curves of HKUST-1 synthesized with precursor solution, [Cu] = 0.12 M, for different reaction times.

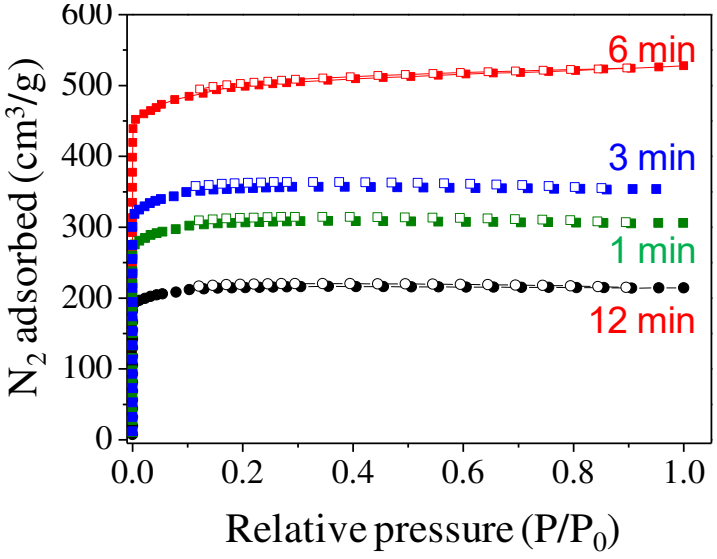

Figure S6. BET nitrogen sorption curves of HKUST-1 synthesized with precursor solution, [Cu] = 0.60 M, for different reaction times.

The powder X-ray diffraction patterns of Co_3BTC_2, Ni_3BTC_2, Co_3BTC_2@Ni_3BTC_2 obtained from both conventional and microfluidic approach

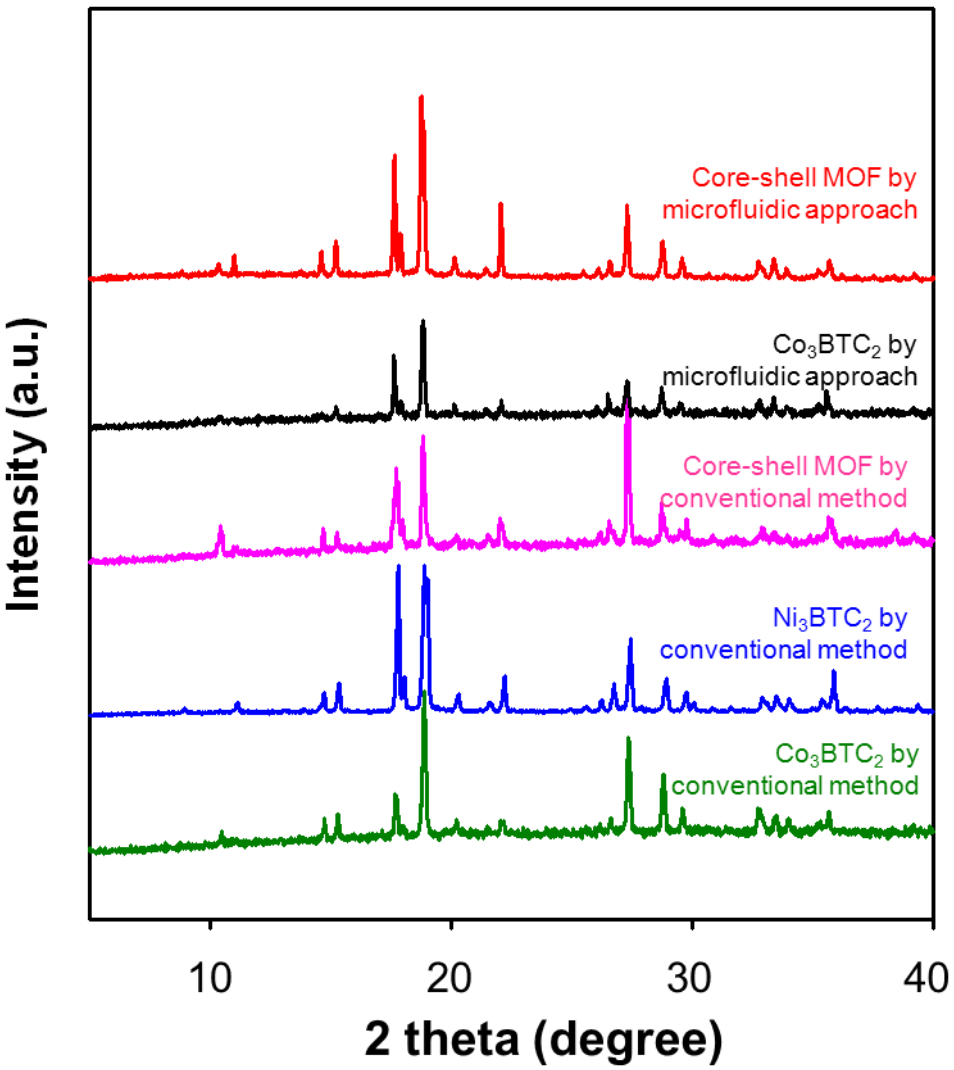

Figure S7. Powder X-ray diffraction patterns of Co_3BTC_2, Ni_3BTC_2 and Co_3BTC_2@Ni_3BTC_2 obtained from both conventional and microfluidic approach.

^{1}H-NMR spectra of the core-shell MOF-5@diCH$_3$-MOF-5 structure

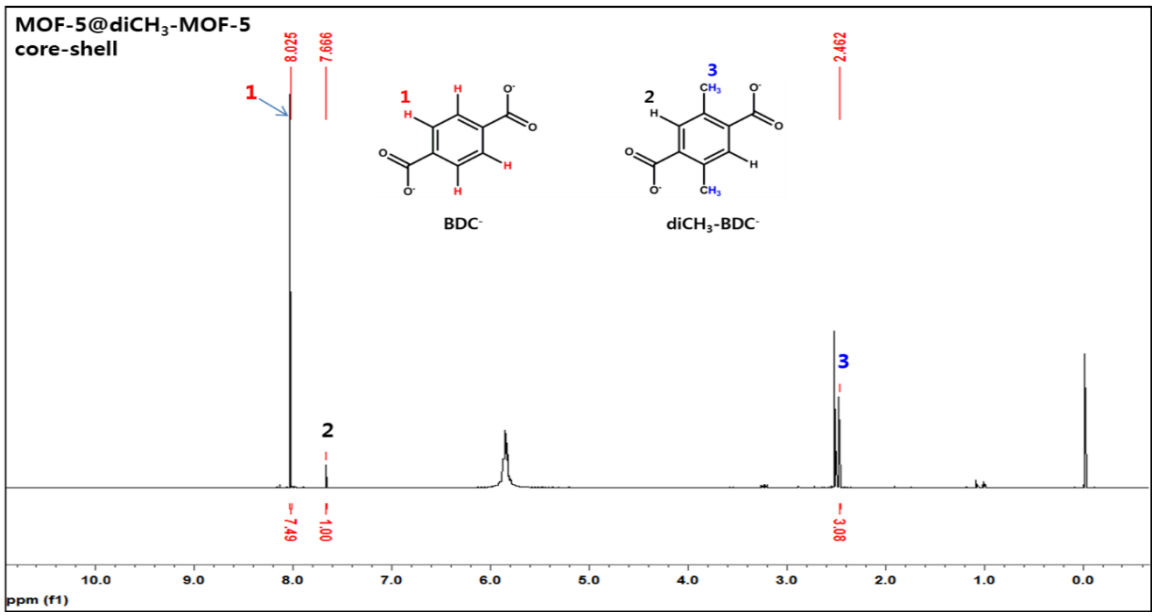

Figure S8. ^{1}H-NMR spectra of the MOF-5@diCH$_3$-MOF-5.

The powder X-ray diffraction patterns of MOF-5 before and after exposure to humid air

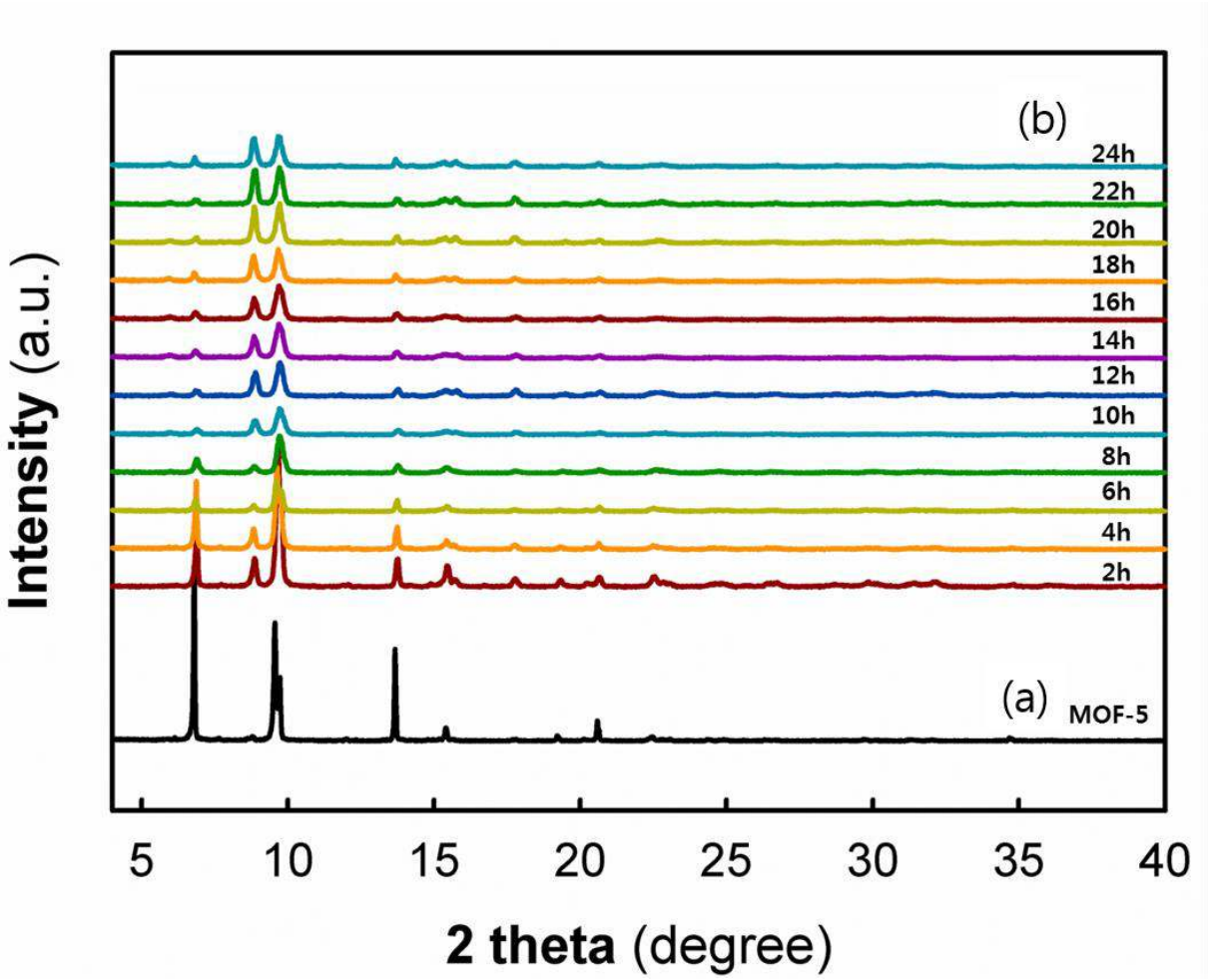

Figure S9. Powder X-ray diffraction patterns of the (a) bare MOF-5 and (b) MOF-5 upon exposure to humid air by differentiation time (from 2 h to 24 h).

Catalytic performance of Fe_3O_4@ZIF-8 for Knoevenagel condensation

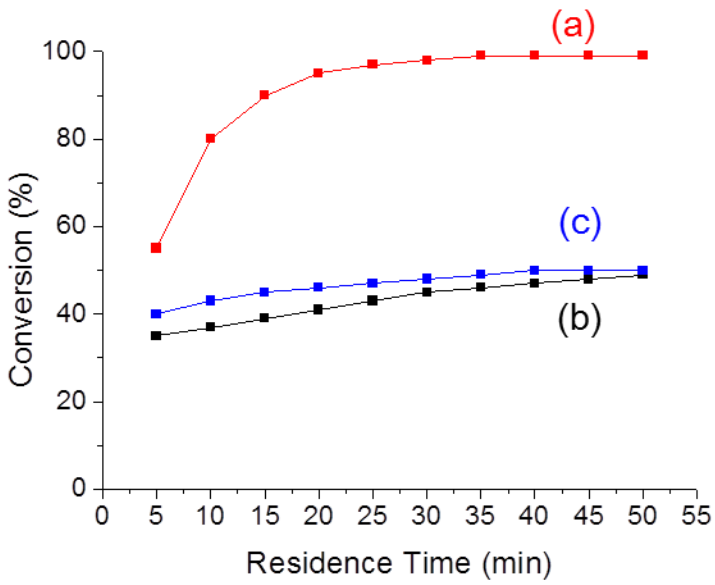

Figure S10. Comparative conversion of benzaldehyde as a function of reaction times by various reaction systems: (a) capillary microreactor, (b) batch reactor and (c) reported data by batch reactor.[S2]

Separation of magnetic Fe_3O_4@ZIF-8

Figure S11. Facile separation of Fe_3O_4@ZIF-8 in the solution using external magnet.

Reference

(S1) Asthana, A.; Kim, K. O.; Perumal, J.; Kim, D. M.; Kim, *Lab Chip*. **2009**, *9*, 1138.
(S2) Zhang, T.; Zhang, X.; Yan, X.; Kong, L.; Zhang, G.; Liu, H.; Qiu, J.; Yeung, K. L. *Chem. Eng. J.* **2013**, *228*, 398.